SANDIA REPORT
SAND2011-9306
Unlimited Release
Printed November 2011

Reference Model 2: “Rev 0” Rotor Design

Matt Barone, Todd Griffith, and Jonathan Berg

Prepared by
Sandia National Laboratories
Albuquerque, New Mexico 87185 and Livermore, California 94550

Sandia National Laboratories is a multi-program laboratory managed and operated by Sandia Corporation, a wholly owned subsidiary of Lockheed Martin Corporation, for the U.S. Department of Energy’s National Nuclear Security Administration under contract DE-AC04-94AL85000.

Approved for public release; further dissemination unlimited.

Sandia National Laboratories

Issued by Sandia National Laboratories, operated for the United ***S***tates Department of Energy by Sandia Corporation.

NOTICE: This report was prepared as an account of work sponsored by an agency of the United States Government. Neither the United States Government, nor any agency thereof, nor any of their employees, nor any of their contractors, subcontractors, or their employees, make any warranty, express or implied, or assume any legal liability or responsibility for the accuracy, completeness, or usefulness of any information, apparatus, product, or process disclosed, or represent that its use would not infringe privately owned rights. Reference herein to any specific commercial product, process, or service by trade name, trademark, manufacturer, or otherwise, does not necessarily constitute or imply its endorsement, recommendation, or favoring by the United States Government, any agency thereof, or any of their contractors or subcontractors. The views and opinions expressed herein do not necessarily state or reflect those of the United States Government, any agency thereof, or any of their contractors.

Printed in the United States of America. This report has been reproduced directly from the best available copy.

Available to DOE and DOE contractors from
U.S. Department of Energy
Office of Scientific and Technical Information
P.O. Box 62
Oak Ridge, TN 37831

Telephone:	(865) 576-8401
Facsimile:	(865) 576-5728
E-Mail:	reports@adonis.osti.gov
Online ordering:	http://www.osti.gov/bridge

Available to the public from
U.S. Department of Commerce
National Technical Information Service
5285 Port Royal Rd.
Springfield, VA 22161

Telephone:	(800) 553-6847
Facsimile:	(703) 605-6900
E-Mail:	orders@ntis.fedworld.gov
Online order:	http://www.ntis.gov/help/ordermethods.asp?loc=7-4-0#online

SAND2011-9306
Unlimited Release
Printed November 2011

Reference Model 2:
"Rev 0" Rotor Design

Matt Barone, Todd Griffith, and Jonathan Berg
Sandia National Laboratories
P.O. Box 5800
Albuquerque, New Mexico 87185-1124

Abstract

The preliminary design for a three-bladed cross-flow rotor for a reference marine hydrokinetic turbine is presented. A rotor performance design code is described, along with modifications to the code to allow prediction of blade support strut drag as well as interference between two counter-rotating rotors. The rotor is designed to operate in a reference site corresponding to a riverine environment. Basic rotor performance and rigid-body loads calculations are performed to size the rotor elements and select the operating speed range. The preliminary design is verified with a simple finite element model that provides estimates of bending stresses during operation. A concept for joining the blades and support struts is developed and analyzed with a separate finite element analysis. Rotor mass, production costs, and annual energy capture are estimated in order to allow calculations of system cost-of-energy.

CONTENTS

INTRODUCTION 7

PRELIMINARY ROTOR SIZING.. 8

ROTOR PERFORMANCE CODE.. 9
  Modifications to the CACTUS Code 9
  Performance Code Validation 11

ROTOR DESIGN 13
  Operating Conditions and Design Load Cases... 13
  Selection of Solidity and Rotational Speed... 14
  Performance and Loads Analysis.. 17
  Blade and Strut Structural Analysis 19
  Blade Design 20
  Strut Design... 22
  Blade/Strut Attachment Design... 23
  Tee/Semi-Blade Joint Design.. 23
  Strut/Tee Joint Design.. 24
    Component Weight... 25

ROTOR COST ESTIMATE.. 25
  Summary of Rotor Cost Model Inputs 26

REFERENCES 27

FIGURES

Figure 1. Schematic of the Reference Model 2 straight-bladed cross-flow turbine. 8
Figure 2. VAWT-850 schematic and photograph of the blade/strut attachment. 12
Figure 3. Measured and predicted rotor performance for the VAWT 850, 13.62 RPM................13
Figure 4. Surface current speed probability distribution, daily averages in 0.1 m/s bins. 14
Figure 5. Water surface level correlated with river current speed. 14
Figure 6. Reference Model 2 blade planform. 15
Figure 7. Dependence of estimated root bending stress on rotor solidity and rotational speed for the extreme operating condition. 15
Figure 8. Rotational speed schedule. 16
Figure 9. Single rotor power curve (no drive train losses). 17
Figure 10. Blade loads at the extreme operating condition. (a) Hydrodynamic normal force distribution on a blade at 54 degrees azimuth. (b) Variation of total blade normal force with azimuth...18
Figure 11. Blade stress distribution. 21
Figure 12. Blade/strut attachment design...23
Figure 13. Shear stress at the tee/blade joint...24

TABLES

Table 1. Rotor Design Parameters. 9
Table 2. Blade Geometry. 16
Table 3. Rotor Performance. 18
Table 4. Material Property Data Selected from SNL/MSU Database. 19
Table 5. Blade Thickness Distribution (root = 0 m and tip = 2.42 m)...21
Table 6. Strut Thickness Distribution (root = 0 m and blade attachment point = 3.23 m). 22

INTRODUCTION

This document summarizes the preliminary design for the cross-flow turbine rotor for Reference Model 2. Reference Model 2 consists of two counter-rotating cross-flow turbines operating at variable rotational speed, and mounted on a floating platform in a riverine environment.

The energy extracting device for Reference Model 2 is a cross-flow turbine, defined as a turbine in which the axis of rotation is perpendicular to the free stream flow. There are several options for selecting a cross-flow turbine configuration, with significant variation in design details amongst the main options. The most efficient and, therefore, the most viable configurations are lift-based devices; that is, they generate torque through the action of lift forces on the rotor blades. Other concepts generate torque through the action of aerodynamic drag on cups or buckets, an example of which is the Savonius rotor. Drag devices are generally not as aerodynamically or structurally efficient as lift-based devices. Amongst lift-based cross-flow turbines, two configurations that were explored extensively for wind energy are the Darrieus turbine and the straight-bladed-Vertical Axis Wind Turbine (VAWT). The Darrieus turbine is comprised of one or more curved blades rotating about a central shaft, with the blade ends affixed to the shaft. The straight-bladed VAWT uses one or more straight blades attached to a central shaft via one or more cantilevered support struts per blade.

A survey of marine hydrokinetic (MHK) industry concepts and prototypes reveals variations on both the Darrieus and the straight-bladed VAWT configurations. Unofficially, the most popular configuration appears to be the straight-bladed machine, a version of which is shown schematically in Figure 1. The turbine rotor consists of a number of straight blades attached to a vertical shaft via support struts. This turbine rotor has a height, H, a diameter, D, radius R, and the aspect ratio is defined as $AR=H/R$.

The straight-bladed turbine has the advantages of simplicity of manufacture and maximization of capture area for a given maximum radius, while it has the disadvantages of larger blade bending loads and aerodynamic losses associated with blade tips and with struts that extend to the maximum radius. Given the apparent popularity of the straight-bladed cross-flow turbine for MHK applications, it is the initial device choice for Reference Model 2. Curved-bladed Darrieus rotor concepts may be explored at a later stage.

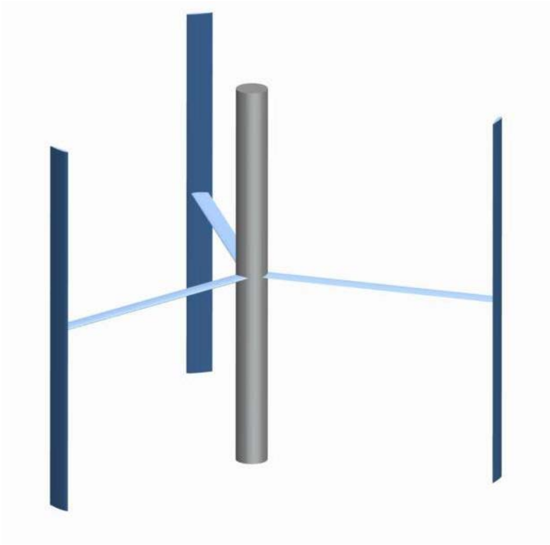

Figure 1. Schematic of the Reference Model 2 straight-bladed cross-flow turbine.

PRELIMINARY ROTOR SIZING

As a starting point for this design exercise, a turbine power rating of 50 kW at 2.0 m/s is specified. This value for power should lead to manageable device sizes, deployable in array configurations. It also represents a reasonable prototype or initial product design scale, suitable for deployment within a range of riverine sites. A baseline aspect ratio of 1.5 is selected. This was (approximately) the aspect ratio employed for the United Kingdom (UK) straight-bladed research VAWT program, which represents the most mature historical straight-bladed VAWT development project (Clare and Mays 1982; Mays, Morgan, Anderson, and Powles 1990). By comparison, the Encurrent straight-bladed MHK device has an aspect ratio of 1.0 (Ginter and Bear 2009). Future design work should explore optimal aspect ratio for the present configuration.

The design rotor thrust coefficient, defined as the non-dimensional force exerted by the fluid on the rotor in the direction of the flow, is initially assumed to be 0.8.

Another key design parameter is the operating depth of the rotor, which dictates shaft length and will influence loads on the power takeoff and platform/mooring systems. We assume, as a starting point, that the center of the rotor is one blade length beneath the water surface (thus, the blade tips will be one half blade length beneath the surface). This parameter should be varied and the effects of proximity to the surface on performance and system loads should be studied in the future.

The initial design parameters from Table 1 define the rotor scale. Additional design details also include the number of blades, the solidity of the rotor, and the hydrofoil sections employed for the blades and the struts. The number of blades, N, is chosen as three. This choice was made to avoid the anticipated dynamic rotor instabilities associated with two-bladed designs. The solidity is defined as $\sigma = {}^{Nc}/_{R}$, where c is the blade chord and R is the rotor radius. More solid rotors are able to withstand higher hydrodynamic loads and may generate more power, but require more material to manufacture. A range of solidities was considered along with a range of maximum operating rotational speeds. This parametric study is described in more detail below. The blade hydrofoil and strut sections use the NACA 0021 foil. The four-digit symmetric NACA foils are commonly used for many applications, and provide simple symmetric sections for which abundant experimental performance data exist. The detailed design choices such as hydrofoil section may be updated and improved in future studies as the rotor is optimized. In this stage of the project, the initial choices allow for baseline rotor performance and weight estimates to be made.

Table 1. Rotor Design Parameters.

Rotor Height (Blade Length)	4.84 m
Rotor Diameter	6.45 m
Rotor Swept Area	31.25 m^2
Rotor Drag Force	50 kN

ROTOR PERFORMANCE CODE

The CACTUS (Code for the Analysis of Cross- and axial-flow TUrbine Simulation) turbine performance code was used for hydrodynamic design of the turbine rotor. CACTUS is an improved version of the original VDART3 code, which was developed during the Sandia National Laboratories VAWT research program. It is currently under development as part of the Department of Energy Water Power Program. It has been modified to handle arbitrary blade geometry so that the straight-bladed turbine can be modeled.

Modifications to the CACTUS Code

Several aspects of the present rotor configuration required modifications to the CACTUS code.

Of critical importance in modeling the performance of a straight-bladed cross-flow turbine is the correct modeling of the parasitic drag of the support struts and strut/blade attachment points. This is especially true at high tip-speed ratios, where the efficiency of the machine is primarily determined by drag losses. In order to capture parasitic drag effects, simple models were implemented into the CACTUS code to account for strut drag and blade/strut attachment drag.

The strut drag model is based on empirical formulations for the profile drag (or drag at zero lift) of streamlined foil sections (Hoerner 1965). The assumption is made that the struts operate at zero angle of attack, which will be true in steady state operation. In practice, inflow turbulence velocity fluctuations in the direction normal to the current direction may induce lift and some additional drag. The profile drag of a foil at incompressible speeds is primarily a function of chord Reynolds number. Well below the critical Reynolds number associated with the onset of boundary layer transition, the sectional drag coefficient is given by

$$C_{d_l} = 2C_{f_l}\left(1+\frac{t}{c}\right)+\left(\frac{t}{c}\right)^2,$$

where $C_{f_l}$is the laminar skin friction force coefficient on a flat plate,

$$C_{f_l} = \frac{2.66}{\sqrt{Re_c}}.$$

Well above the critical Reynolds number, the sectional profile drag coefficient is estimated by

$$C_{d_t}\Big/2\,C_{f_t} = 1 + 2\,\frac{t}{c} + 60\left(\frac{t}{c}\right)^4,$$

where

$$C_{f_t} = \frac{0.044}{(Re_c)^{1/6}}.$$

The critical Reynolds number, Re_{crit}, is chosen as 3×10^5, which is approximately the chord Reynolds number midway between the onset of transition and achievement of attached transitional flow for foils of moderate thickness. The sectional drag for a given chord Reynolds number is calculated using a smooth blending function of the laminar and turbulent expressions:

$$C_d = \big(1 - f(Re_c)\big)C_{d_l} + f(Re_c)C_{d_t}$$

$$f(Re_c) = \frac{1}{2}\left(1 + tanh\left[\frac{\log_{10} Re_c - \log_{10} Re_{crit}}{0.2}\right]\right).$$

Within CACTUS, the blade struts are divided into a number of elements, each of which generates a drag force according to the above formulae. The local Reynolds number and dynamic pressure are calculated from the local velocity magnitude, which includes contributions from the free-stream and the induced velocity of the blades and rotor wake. The drag force is then multiplied by the radius of the strut element to calculate the decrement in torque due to the parasitic drag.

The interference drag due to the blade/strut attachment, or junction, point is approximated using the empirical relation for a t-junction of two foils (Hoerner 1965):

$$C_{d_j} = \left(\frac{t}{c}\right)^2\left(17.0\,\left(\frac{t}{c}\right)^2 - 0.05\right).$$

The thickness-to-chord ratio is taken as the average of the blade and strut chords at the attachment point. The reference area for the junction drag coefficient is the square of the local chord.

Additional parasitic drag may result from interference drag not captured by the simple t-junction formula, drag from other parts of the blade-strut fitting, and/or manufacturing defects on the blade or strut surface. This can be accounted for using an arbitrary parasitic drag coefficient, $C_{d_{par}}$, with reference area equal to the square of the equatorial blade chord.

The twin counter-rotating rotor configuration introduces turbine-turbine interactions due to the close proximity of the rotors. CACTUS is currently a single-rotor analysis code; however, with minimal modification it is able to model a special case of the dual-rotor configuration. If the rotor azimuthal position is in phase, then the effect of one rotor on the other is modeled as a symmetry condition on the plane containing the free stream velocity vector that is located midway between the axes of rotation. This condition is expected to provide reasonable predictions of turbine wake interaction effects for inter-rotor spacings of at least one half of a rotor diameter. Closer spacings likely will involve strong interaction of the rotor wakes close to the blades, and turbulent mixing may need to be modeled in order to accurately capture the interaction effects.

Performance Code Validation

A literature survey of validation data for straight-bladed cross-flow turbines pointed to the UK VAWT research program of the 1980s and early 1990s. A series of research turbines based on the straight-bladed design were built and tested, culminating in the construction of a 500 kW demonstration turbine at the UK Carmarthen Bay Wind Turbine Demonstration Centre. This turbine, dubbed the VAWT 850 due to its swept area of 850 m^2, was undergoing commissioning when preliminary performance data were published in September 1990.

The turbine rotor consisted of two blades, attached at mid-span to a crossarm member, which connected the blades to the top of a central tower containing the rotor bearing and drive train (see Figure 2). The blades were 24.3 m long, and tapered such that the tip chord was 75% of the mid-span chord. The mean chord of the blades was 1.75 m. The blade foils were NACA0018 sections, while the crossarm consisted of an outer section with NACA0030 cross section and an inner section with an elliptical cross section. For this study the crossarm is modeled as a constant chord member with NACA0030 section along its entire length and chord equal to the blade mid-span chord. Hub height for the machine was 30 m, and the diameter was 35 m. The rated power of the machine was 500 kW at a rotational speed of 20.4 RPM, although published performance data are apparently only available for a rotational speed of 13.62 RPM.

The published power curve gives generator power versus wind speed. In order to compare the data with numerical predictions, the generator is converted to a rotor power using an assumed drive train efficiency of 90%. This assumption and the associated uncertainty in experimental rotor power should be considered when comparing the data to the predictions. Another source of uncertainty is the interference drag due to the blade-strut attachment and its associated hardware (see photograph in Figure 2). The empirical relations described earlier were used to model the crossarm drag and the attachment interference drag. An additional parasitic drag with a drag coefficient of 0.2 based on the square of the blade chord at the attachment point was also added. The value of 0.2 was chosen so that good agreement between predictions and data was obtained at high tip-speed ratios. A better approach would be to estimate the parasitic drag from experimental characterization of the machine; however, in this case such data did not exist. This test case highlights the critical importance of characterizing blade-strut attachment drag for accurate prediction of cross-flow turbine performance.

CACTUS simulations of the VAWT 850 were performed at the 13.62 RPM operating condition for which data were available. The model incorporated 16 blade elements per blade, and 20 time steps per rotor revolution. A total of 15 revolutions were simulated for tip-speed ratios of less than 4, and 25 revolutions were simulated for higher tip speeds. The modified Boeing-Vertol dynamic stall model was used in these simulations. Figure 3 compares the experimental data for rotor power and power coefficient to CACTUS predictions. Very good agreement is obtained for the Cp curve, although it should be stressed that the parasitic drag was chosen to ensure good agreement at high tip-speed ratio. The stall wind speed and power level at stall is well-predicted, but the post-stall power is underpredicted at higher wind speeds. These results indicate room for improvement in the dynamic stall model. Overall, the agreement with experiment is sufficiently good such that CACTUS can be used with confidence as a design tool for straight-bladed cross-flow turbines.

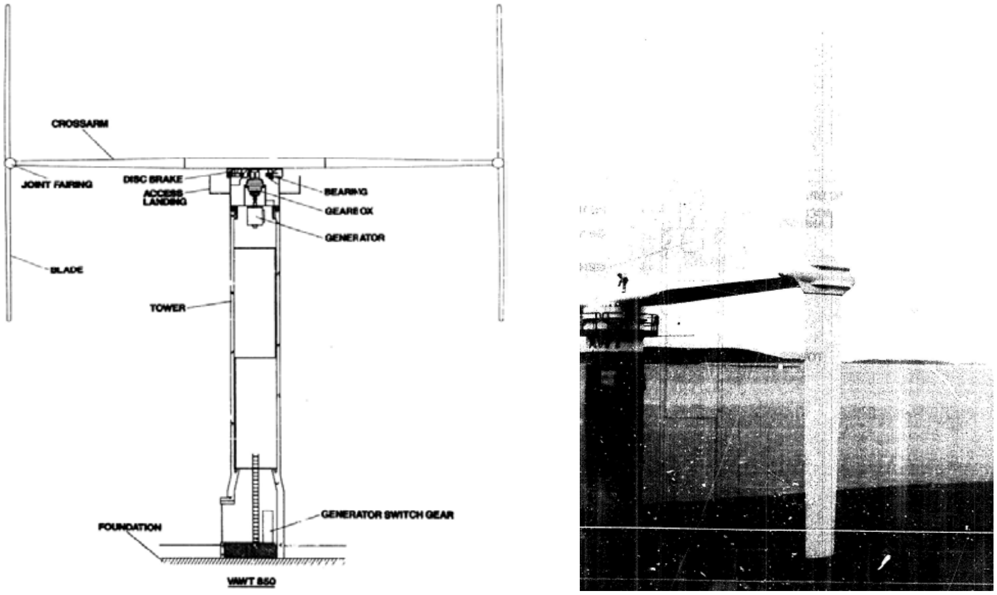

Figure 2. VAWT-850 schematic and photograph of the blade/strut attachment.

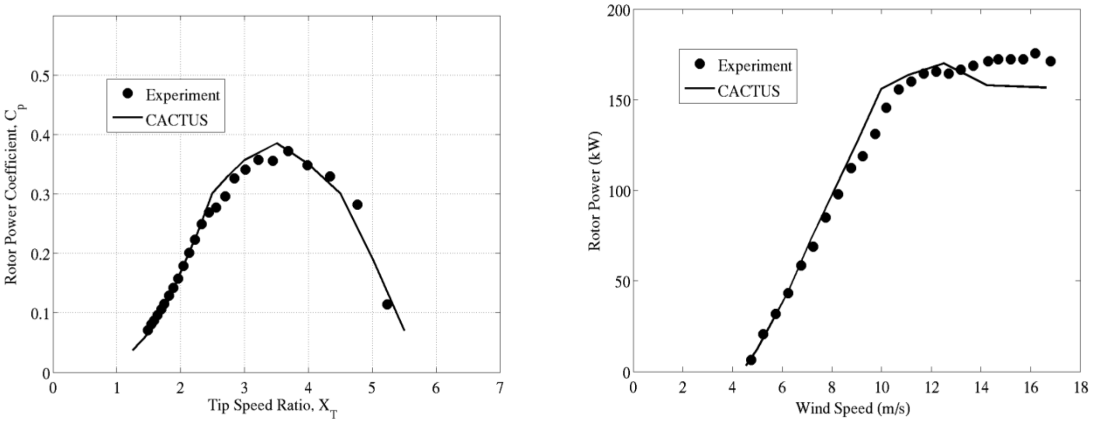

a) Power coefficient vs. tip speed ratio

b) Power vs. wind speed

Figure 3. Measured and predicted rotor performance for the VAWT 850, 13.62 RPM.

ROTOR DESIGN

Operating Conditions and Design Load Cases

Operating parameter ranges and design load cases for the rotor are specified according to the reference model site characteristics. The probability density distribution of surface current velocity for the site in bins of 0.1 m/s is shown in Figure 4. Based on this distribution, the cut-in current speed of the turbine is specified as 0.7 m/s, and the cut-out speed is 2.6 m/s. The 50-year and 100-year return surface velocities are 2.81 m/s and 2.92 m/s, respectively. The maximum surface current speed during turbine operation is specified as 25% higher than the cut-out speed, corresponding to an extreme “gust” event with a short rise time such that the turbine control system is unable to slow the rotor quickly enough to alleviate the load. This extreme surface current speed is 3.25 m/s. This design case is termed the extreme operating load case, and is the design driver for the rotor. A parked load case with instantaneous surface current speed of 25% greater than the 50-year return velocity, or 3.51 m/s, was also considered. In the parked load case, the blades are assumed to be stationary and the drag force on the blades is predicted using empirical flat plate drag relations. The out-of-plane bending loads for the extreme operating load case were found to be much greater than those for the parked load case.

The water surface level of a river is correlated with the river current speed, with larger current speeds associated with larger water surface levels. This relationship was defined for the reference site and is shown in Figure 5(a). The mean velocity profile is given as a function of distance from the river bed normalized by the water surface level in Figure 5(b). This is a power law profile, with exponent of 1/6, which was found to be representative for large river sites in the United States. Both of these site characteristics are included in the CACTUS performance and load simulations.

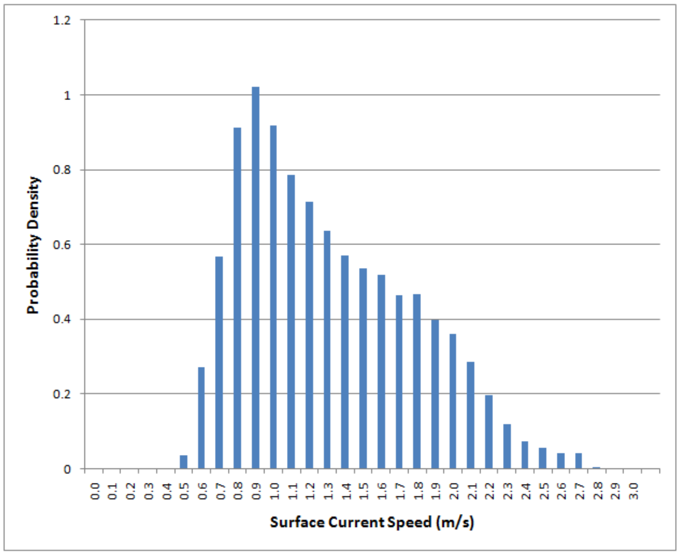

Figure 4. Surface current speed probability distribution, daily averages in 0.1 m/s bins.

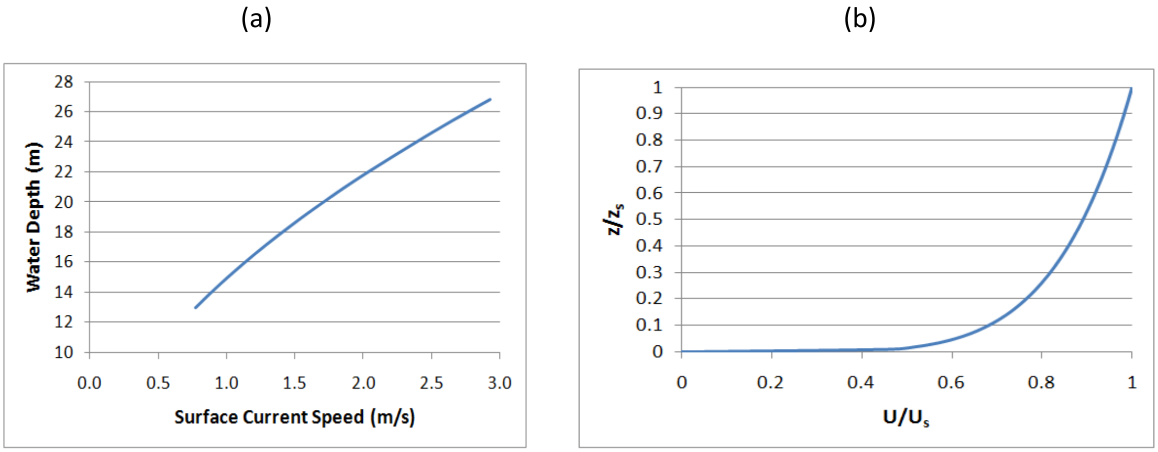

Figure 5. Water surface level correlated with river current speed.
(a) Relationship between water depth at deployment location
and surface current speed. (b) Power law velocity profile with exponent of 1/6.

Selection of Solidity and Rotational Speed

Initial design iteration assuming a constant-chord blade planform suffered from unacceptably high blade root bending stresses. Two methods to alleviate these stresses were considered: adding a second support strut, or tapering the blade. A second support strut was considered undesirable and to be avoided if possible, given the high performance penalty associated with struts. Blade taper proved to be an effective means of increasing structural strength near the root with a relatively modest performance penalty associated with the thicker mid-span sections. The chord is linearly tapered such that the tip chord is 75% of the root chord (here, “root” and “mid-span” are used interchangeably). The blade planform shape is shown in Figure 6.

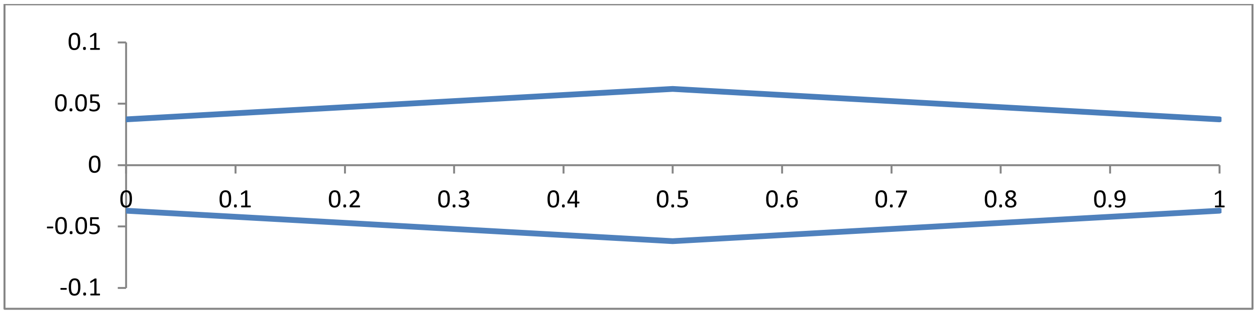

Figure 6. Reference Model 2 blade planform.

Rotor solidity and rotational speed were selected based on the extreme operational load case. Figure 7 shows the estimated maximum root bending stress as a function of rotational speed for this design case. These stresses were estimated by applying loads predicted by CACTUS to a simple beam model for the blade, with an assumed root sectional stiffness. The allowable stress is 282 MPa (see later section on blade structural design for material description). In order to provide some margin due to the approximate method for determining root bending stress, a maximum RPM of 14 was selected with a solidity of 0.3. The final nondimensional blade chord distribution is given in Table 2.

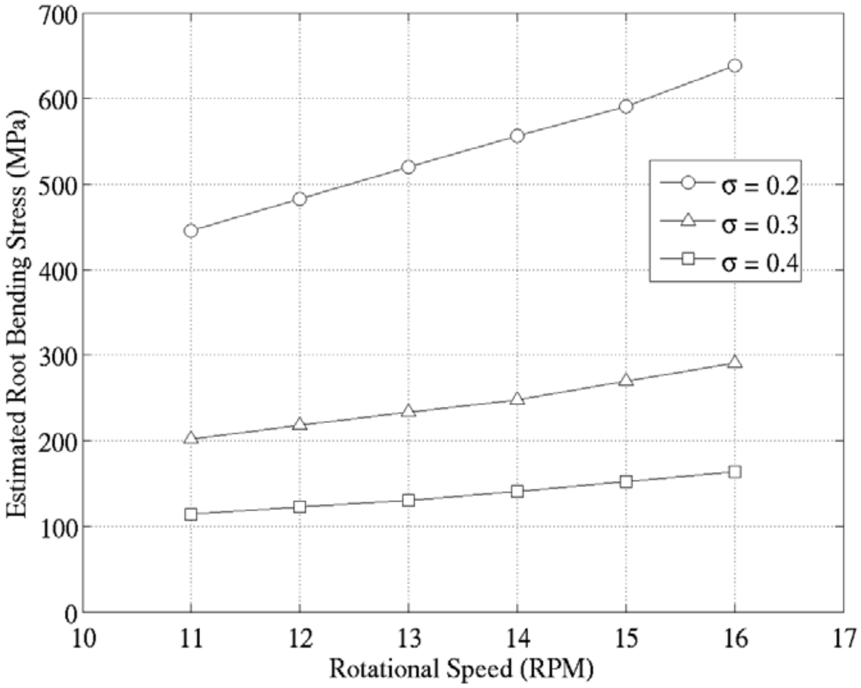

Figure 7. Dependence of estimated root bending stress on rotor solidity and rotational speed for the extreme operating condition.

Table 2. Blade Geometry.

Spanwise Coordinate y/H	**Chord c/R**
-0.5	0.0744
-0.4	0.0843
-0.3	0.0943
-0.2	0.1042
-0.1	0.1141
0.0	0.1240
0.1	0.1141
0.2	0.1042
0.3	0.0943
0.4	0.0843
0.5	0.0744

The rotational speed is thus limited by the extreme load to below the optimum for high current speeds. However, as current speed decreases, the optimal tip-speed ratio is approached. As current speed decreases below this value, the rotational speed is then decreased to approximately follow the optimal tip-speed ratio down to cut-in (see Figure 8).

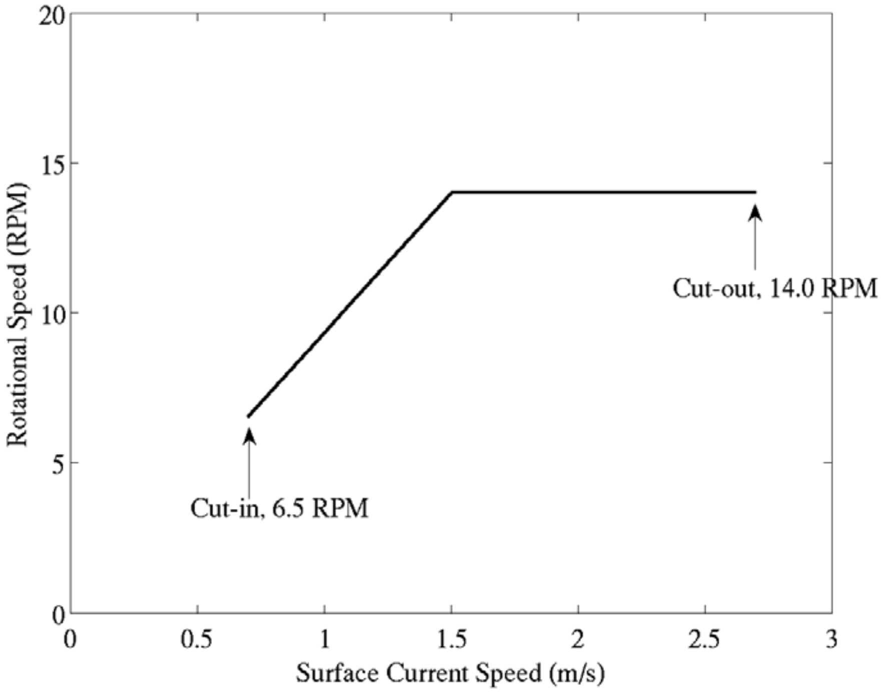

Figure 8. Rotational speed schedule.

Performance and Loads Analysis

CACTUS simulations were run for the operational current speed range, in 0.1 m/s increments in order to generate a power curve. These simulations incorporated the sheared velocity profile corresponding to each current speed. The single machine rotor power curve is shown in Figure 9 and tabulated in Table 3. Dual-rotor power was estimated for the tandem counter-rotating rotor configuration by application of a symmetry boundary condition in CACTUS. The turbine-turbine interaction at a separation distance (blade-to-blade) of one radius resulting in a minor decrease in predicted rotor performance. A uniform drive train efficiency of 90% was used to estimate generator power. The power curve and the given velocity distribution were combined to estimate annual energy production of 274.2 MW-hr for the dual-rotor system. This corresponds to a capacity factor of 0.31 (using a machine rating of 51 kW).

A CACTUS simulation at the extreme operating load condition of 3.25 m/s current speed was used to generate the design hydrodynamic flap-wise loads for the blade structure. Figure 10 shows the blade normal force distribution for the blade azimuth position where normal forces are largest. Also shown is the variation of total blade normal force with blade azimuth. In-plane (or edge-wise) loads are significantly lower than the flap-wise loads, and are not expected to constrain the blade structural design. Loads on the blade strut are not calculated in CACTUS. The load condition for the struts was assumed to derive from a uniform “gust” with vertical velocity equal to 25% of the current speed during a parked condition with surface current speed of 3.5 m/s. This was estimated to produce a uniform 3-kilonewton (kN)/m flap-wise load distribution on the strut.

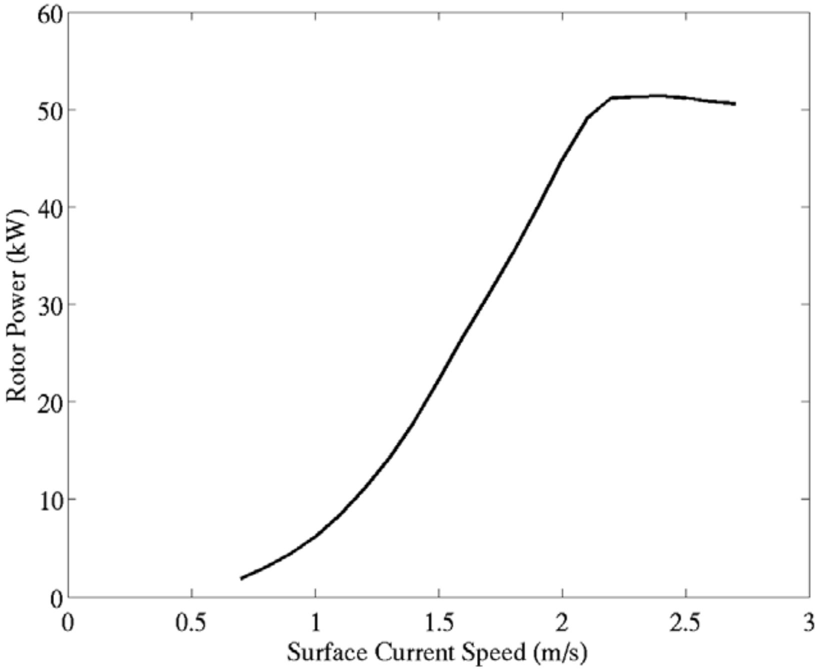

Figure 9. Single rotor power curve (no drive train losses).

Table 3. Rotor Performance.

Current Velocity (m/s)	**Rotor Speed (rmp)**	**TSR**	**Rotor Power (kW)**
0.7	6.53	3.15	2.4
0.8	7.46	3.15	3.6
0.9	8.39	3.15	5.2
1.0	9.33	3.15	7.3
1.1	10.26	3.15	9.8
1.2	11.19	3.15	12.8
1.3	12.13	3.15	16.4
1.4	13.06	3.15	20.7
1.5	14.00	3.15	25.6
1.6	14.00	2.96	30.1
1.7	14.00	2.78	34.3
1.8	14.00	2.63	38.8
1.9	14.00	2.49	43.9
2.0	14.00	2.36	48.5
2.1	14.00	2.25	51.1
2.2	14.00	2.15	51.5
2.3	14.00	2.06	51.4
2.4	14.00	1.97	51.1
2.5	14.00	1.89	50.8
2.6	14.00	1.82	50.7
2.7	14.00	1.75	49.5

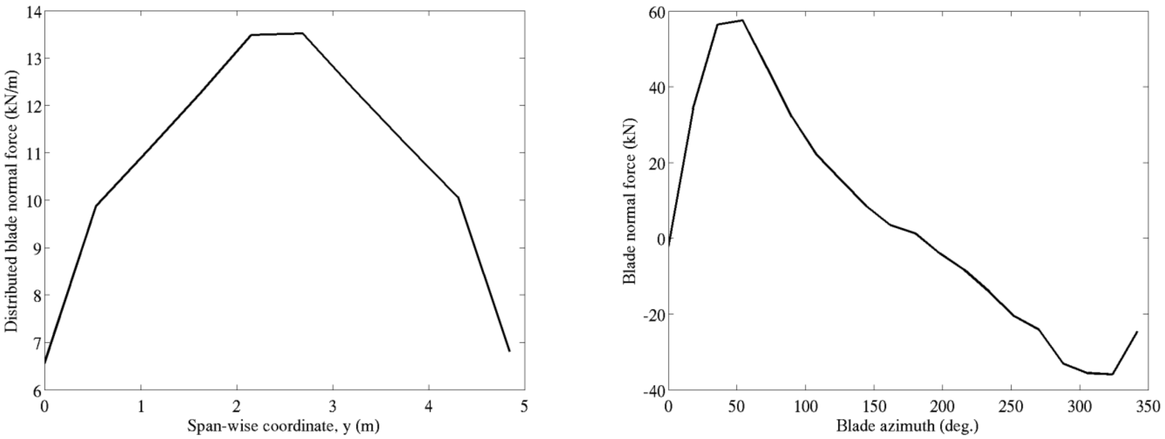

Figure 10. Blade loads at the extreme operating condition. (a) Hydrodynamic normal force distribution on a blade at 54 degrees azimuth. (b) Variation of total blade normal force with azimuth.

Blade and Strut Structural Analysis

With focus on rotor cost estimation, blade and struts were designed. An extreme loading condition described in a previous section was analyzed. Glass-only materials were utilized to reduce material cost. In the end, it was determined that a high fraction of unidirectional materials were needed along with thick laminates to resist the loads.

Table 4 lists properties for the unidirectional and double-bias materials. Elastic properties and ultimate stress for the blade/strut laminates were determined by rule of mixtures with 90% unidirectional and 10% double-bias. Rule of mixtures is essentially a weighted average of the properties, and is commonly used to estimate elastic properties. Based on experience, the rule of mixtures provides a good approximation of single cycle (ultimate) failure stresses as well. Therefore, ultimate tensile and compressive stresses were also computed using the rule of mixtures.

Table 4. Material Property Data Selected from SNL/MSU Database.

Laminate Definition			**Longitudinal Direction**								**Shear**
			Elastic Constants				**Tension**		**Compression**		
VARTM Fabric/resin	**lay-up**	**V_F %**	**E_L GPa**	**E_T GPa**	**υ_{LT}**	**G_{LT} GPa**	**UTS_L MPa**	**ε_{max} %**	**UCS_L MPa**	**ε_{min} %**	**τ_{TU} MPa**
E-LT-5500/EP-3 (“uni”)	$[0]_2$	54	41.8	14.0	0.28	2.63	1151	2.97	-740	-1.79	30
Saertex/EP-3 (“double bias”)	$[\pm45]_4$	44	13.6	13.3	0.51	11.8	144	2.16	-213	-1.80	----
Blade and strut laminate	90% uni, 10% double bias		39.0	13.9	0.3	3.55	1051	n/a	-687	n/a	n/a

E_L – Longitudinal modulus, υ_{LT} – Poisson’s ratio, G_{LT} and τ_{TU} – Shear modulus and ultimate shear stress, UTS_L – Ultimate longitudinal tensile strength, ε_{MAX} – Ultimate tensile strain, UCS_L – Ultimate longitudinal compressive strength, ε_{MIN} – Ultimate compressive strain.

Wind turbine design standards (GL) were used to determine a combined safety factor. A factor for loads of 1.1 was determined for the extreme load condition selected for these analyses, which is considered an abnormal condition. A factor for materials of 2.205 was determined, which assumed state-of-the-art manufacturing and includes aging and temperature effects. Thus, the combined safety factor for materials and loads is 2.43.

For the 90/10 laminate, allowable stresses of 432 MPa (allowable tension) and -282 MPa (allowable compression) are determined from Table 4 using the combined safety factor of 2.43. Of course, compressive stress is the design driver.

Flap-wise loads for the rotor azimuth position with the largest loading (54-degree location) were selected for the blade design. Edge-wise and torsional loads were not considered in this design iteration as the flap-wise loads were considerably larger. Inertial loads were also not included as they were estimated to be small compared to the hydrodynamic loads.

For the strut design, two load scenarios were considered: (1) Land-based fabrication: dry weight of blades and struts during fabrication, and (2) operation: “wet” weight of blades and struts plus hydrodynamic flap-wise loads during operation. The “wet” weight is determined as the dry weight of the blade/strut minus the weight of water displaced by the blade/strut. Hydrodynamic loads were determined by the Cactus code (see the previous section).

Blade Design

To account for the blade/strut attachment joint, it was assumed that the blades were of solid cross section from the blade strut attachment point to 0.807 m along the span. A shell laminate was designed from the 0.807-m span to the blade tip (2.42 m). No shear webs were included in this design. Shell thicknesses along the span were designed conservatively (with respect to local span-wise bending stress) to account for the potential need of additional weight of shear webs that may be needed to prevent shell buckling. A buckling calculation has not been performed for this design, and will be performed once the design and structural model mature to sufficient detail to permit its calculation. Outboard of 0.807 m, a solid blade is not required. Therefore, the shell thickness was determined according to the loads. The PreComp code (Bir 2007) was used to determine the blade cross-section properties for the outboard sections. The resulting tapered half-blade mass was 45.2 kg. For comparison, a solid, tapered half-blade (2.42 m in length) with 0.4-m root chord and 0.24-m tip chord has mass of 63.2 kg. The design root bending moment, corresponding to the maximum load during the extreme operational condition, for the half-blade was 34,437 N-m. The resulting root bending stress was 169 MPa, which is significantly less than the allowable of 282 MPa.

The blade stress distribution along the half-blade span is plotted in Figure 11. The blue curve represents the designed blade with mass of 45.2 kg while the red curve represents a solid blade with 63.2-kg mass. The plot demonstrates that a sizeable stress margin exists with respect to the allowable stress. Future analysis will include fatigue, buckling, and modal analysis that will demonstrate if additional structural optimization/weight reduction is possible. Alternatively, this margin may allow for deployment in more energetic sites than the current reference site.

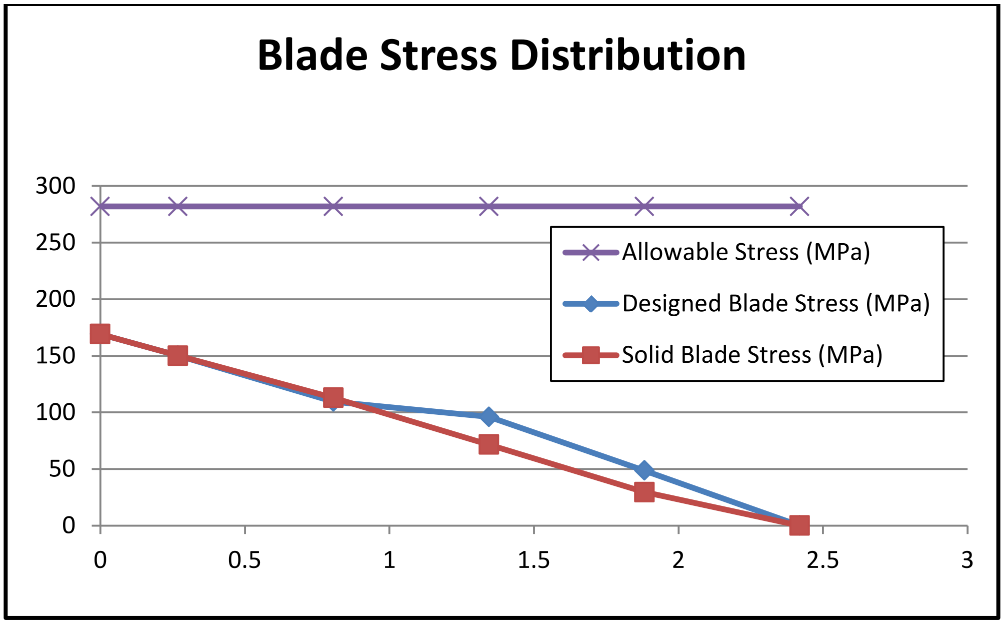

Figure 11. Blade stress distribution.

The half-blade shell thickness is tabulated in Table 5. Span is defined from the root of the half-blade to the tip. Each half-blade is identical above and below the blade/strut attachment location. From 0 to 0.807 m, the blade is of solid cross section. At 0.807 m, a shell of 0.018-m thickness begins. From 0.807 m to 1.344 m, the thickness linearly varies from 0.018 m to 0.012 m. Likewise, from 1.334 m to 1.882 m, the thickness linearly varies from 0.012 m to 0.010 m. From 1.882 m to 2.42 m, the thickness is a constant 0.010 meters.

Table 5. Blade Thickness Distribution (root = 0 m and tip = 2.42 m).

Span (m)	Chord (m)	Shell thickness (m)
0	0.4	Solid
0.269	0.382	Solid
0.807	0.346	0.018
1.344	0.311	0.012
1.882	0.275	0.010
2.42	0.24	0.010

Strut Design

To account for the blade/strut attachment joint as well as the strut/tower attachment joint, the initial 0.25 m at each end of the strut were designed to be of solid cross section. A constant strut chord of 0.36 m was analyzed, which is in line with the current blade/strut attachment joint design (see the next section). The loads that were considered for the strut analysis include a uniform distributed 3-kN/m hydrodynamic load, the weight of the blades at the tip of the strut, and the distributed strut weight. The blade and strut weights were considered for both the dry and wet cases. It was found that the root bending moment for the dry case (land-based fabrication) was 4,454 N-m and for the wet case (during operation) 17,166 N-m. Therefore, the wet case was chosen for analysis. The interior shell, between the solid end sections of 0.25-m length, was designed such that the entire load (17,166 N-m) could be carried at any point along the span (to be conservative). The maximum stress in the shell section was determined to be 149 MPa, which is significantly less than the 282 MPa allowable. The design mass of the strut was 58.8 kg. For comparison, a solid strut would have mass of 100.6 kg.

The strut shell thickness is tabulated in Table 6. Span is defined from the root of the strut (at the strut/tower connection) to the blade/strut attachment. From 0 to 0.25 m, the strut is of solid cross section. At 0.25 m, a shell of 0.010-m thickness begins. From 0.25 m to 2.73 m, the thickness is constant 0.010 m. From 2.73 to 3.23 m, the strut is of solid cross section.

Table 6. Strut Thickness Distribution (root = 0 m and blade attachment point = 3.23 m).

Span (m)	**Chord (m)**	**Shell thickness (m)**
0	0.36	Solid
0.25	0.36	0.010
2.73	0.36	0.010
3.23	0.36	Solid

Blade/Strut Attachment Design

The blade/strut attachment design assumes the strut and two semi-blades will be permanently bonded together with a “tee” joint with mortise-and-tenon connections, as shown in Figure 12. The length of each tenon is about 150 mm and the interface between parts is about 100 mm from the center of the tee joint.

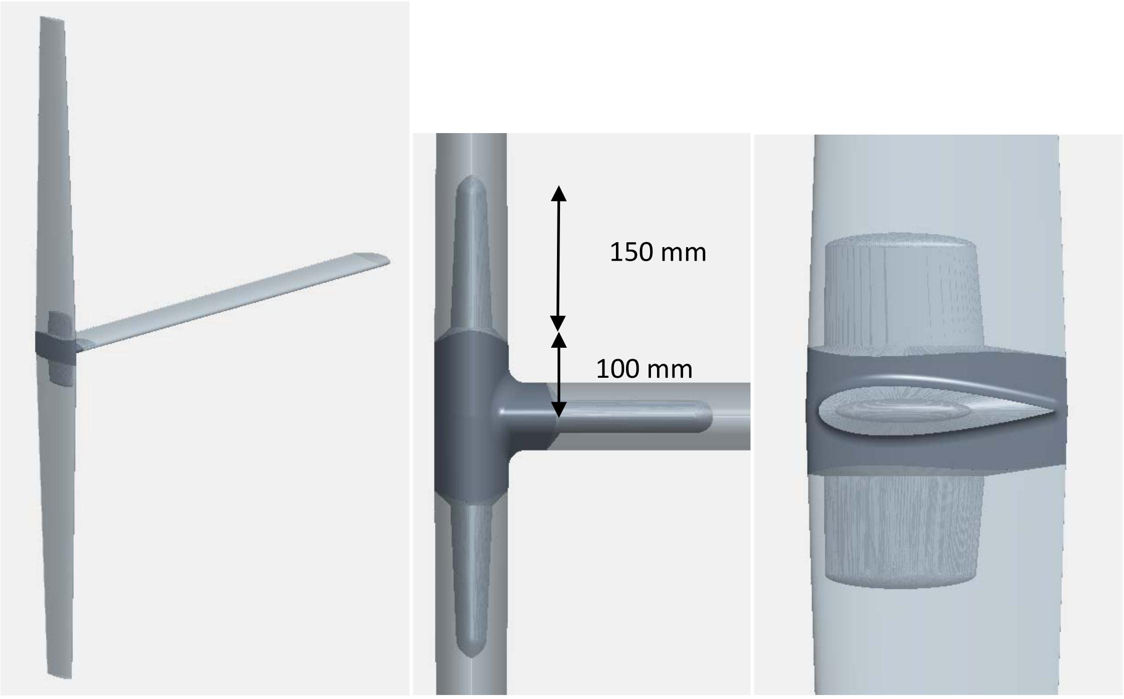

Figure 12. Blade/strut attachment design.

There are two attachments to be analyzed: (1) the strut/tee attachment and (2) the tee/semi-blade attachment.

Tee/Semi-Blade Joint Design

The solid model of one semi-blade was imported into ANSYS for a static analysis. The goal of this analysis was to find the shear stress at the joint surfaces. In future work, the assembly will be analyzed with the adhesive included with appropriate bond thickness. For now, however, the shear stress at the fixed support surfaces will be taken as an approximation of the stress in the adhesive.

The semi-blade was loaded with the maximum hydrodynamic forces of 9 kN in the tangential direction toward leading edge and 29 kN toward the center of rotation. These forces were applied at the approximate load center of 1.72 m from the semi-blade root.

After a *brief* consideration of available adhesives, Plexus MA550 was selected for the first design cycle because this product is classified as a marine adhesive and Plexus adhesives are commonly used to build wind blades. Further attention should be given to selection of the adhesive. Plexus MA550 has a lap shear strength of 8.9 to 12.4 MPa.

Figure 13 shows the shear stress results. For most of joint interface, the shear stress is around 1.1 MPa; however, there are stress concentrations that bring the maximum stress up to 17 MPa. This initial analysis indicates that an all-adhesive joint is feasible, but additional attention is required to stress concentrations in the detailed design.

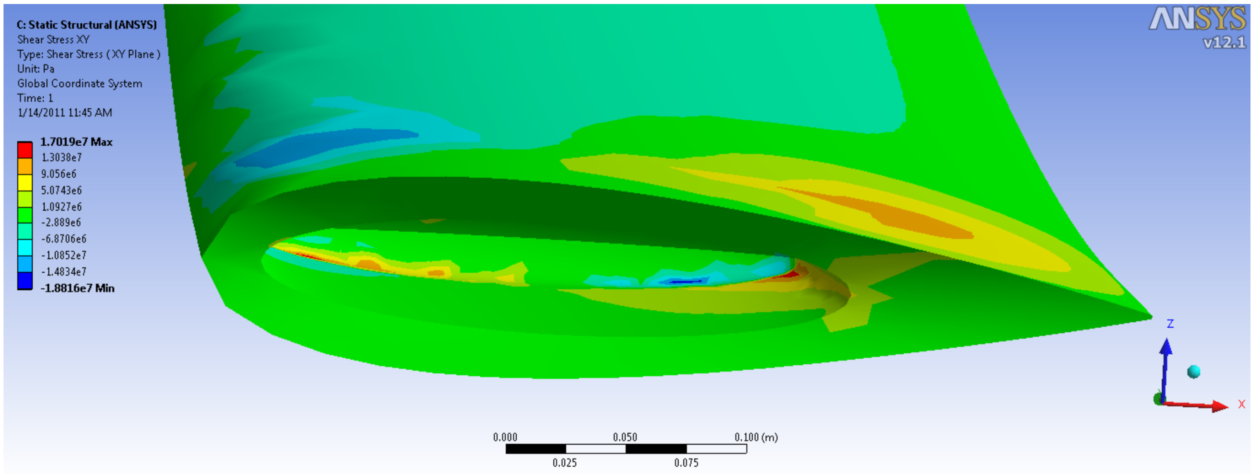
C: Static Structural (ANSYS)
Shear Stress XY
Type: Shear Stress (XY Plane)
Unit: Pa
Global Coordinate System
Time: 1
1/14/2011 11:45 AM
1.7019e7 Max
1.3038e7
9.056e6
5.0743e6
1.0927e6
-2.889e6
-6.8706e6
-1.0852e7
-1.4834e7
-1.8816e7 Min
ANSYS
v12.1
Z
X
0.000
0.050
0.100 (m)
0.025
0.075

Figure 13. Shear stress at the tee/blade joint.

Strut/Tee Joint Design

The strut/tee joint design was analyzed with some basic hand calculations. The highest axial force directed outward is -35.92 kN and occurs at 324 degrees rotor azimuth. The highest axial force directed inward is 57.6 kN and occurs at 54 degrees rotor azimuth.

Centrifugal force assuming a full-blade weight of 2x(45.2 kg) = 90.4 kg and rotor speed of 14 rpm (1.466 rad/s) is

$$F = -mr\Omega^2 = -(90.4)(3.225)(1.466)^2 = -0.63 \text{ kN}.$$

When the axial force on the strut is directed inward, the load is offset by the centrifugal force of the blade weight. When the axial force on the strut is directed outwardly (negative), the axial force and centrifugal force combine to give a greater load. Given the small magnitude of the centrifugal force, we use the 57.6-kN force as the design driver and consider the centrifugal force to be negligible.

The required surface area of the bonded joint can be calculated given the design load and allowable shear stress of the adhesive. We use the same combined safety factor of 2.43 that was used previously.

$$A = SF \times \frac{F_{axial}}{\tau_{allow}} = 2.43 \times \frac{57.6\text{kN}}{8.9\text{ Mpa}} = 0.0157\text{ m}^2 = 15700\text{ mm}^2$$

The bond surface area per longitudinal distance along the strut was calculated for two design cases. It was assumed that the wall thickness for a “mortise-and-tenon” style joint would be between 10 and 20 mm. The surface area per joint length for the two cases is approximately 640 mm^2/mm and 500 mm^2/mm, respectively. Assuming the wall thickness will be closer to 20 mm, the required bond length to withstand axial load is 15700/500 = 32 mm.

Bending loads at the strut to full-blade joint have not been considered in the current analysis. In addition, allowance must be made for defects introduced during assembly. For these reasons, the bond length in the current design has been increased to 150 mm.

Component Weight

The “tee” component has a volume of 0.009 m^3. Assuming fiberglass construction with the 90/10 material specified previously, the mass is 17.2 kg.

ROTOR COST ESTIMATE

The reference model rotor blades and struts can be manufactured using current practice in production of wind turbine blades. This is justified by similarity in materials and in structural shape between the two applications. Half of one cross-flow turbine blade is comparable to a single-axial flow turbine blade, since each is a cantilevered structure with the primary design constraint consisting of resistance of flap-wise loading. Given this similarity, cost modeling employed for wind turbine rotors may be applicable. The WindPACT program developed cost estimates for blade molds, tooling, and production for blades between 40 and 60 meters in length (Griffin 2001). The current reference model involves much smaller blades; the effect of small scale on the rotor cost relationships remains to be assessed. The WindPACT report’s relationship of $10.45/kg (in 2000 currency) is used here to give a rough estimate of the rotor production costs (includes material and labor, but not mold and tooling costs) for the current reference model. Adjusted for inflation, the current production cost in 2010 dollars is $13.38/kg. A mature production run is assumed, such that the learning curve multiplier is unity. Additional cost will be incurred for fabrication of the blade/strut joint hardware. Estimates for this cost will need to be obtained from a suitable manufacturer.

Summary of Rotor Cost Model Inputs

Annual Energy Production (Dual Rotor)	**274.2 MW-hr**
Single Blade Mass	**90.4 kg**
Single Strut Mass	**58.8 kg**
Total Single Rotor Mass (3 Blades + 3 Struts)	**447.6 kg**
Estimated Dual Rotor Production Cost ($13.38/kg)	**$11,980**

REFERENCES

Bir, G., 2007, *NWTC Design Codes (PreComp)*. Retrieved March 26, 2007, from http://wind.nrel.gov/designcodes/preprocessors/precomp/.

Clare, R., and R. C. Mays, 1982, The Musgrove variable geometry vertical-axis wind turbine, *Modern Power Systems*, pp. 35-38.

Ginter, V., and C. Bear, 2009, *Development and application of a water current turbine*, New Energy Corporation, Inc.

Griffin, D. A., 2001, *WindPACT turbine design scaling studies technical area 1 – Composite blades for 80- to 120-meter rotor*, NREL/SR-500-29492.

Hoerner, S. F., 1965, *Fluid Dynamic Drag* (Second ed.). Published by author.

Mays, I. D., C. A. Morgan, M. B. Anderson, and S. R. Powles, 1990, Experience with the VAWT 850 demonstration project, *Proceedings of the European Community Wind Energy Conference*.

DISTRIBUTION

1	MS1124	Matt Barone	6121
1	MS1125	Jonathan Berg	6121
1	MS1124	Todd Griffith	6122
3	MS1124	Richard Jepsen	6122
1	MS0899	RIM–Reports Management	9532 *(electronic copy)*

Sandia National Laboratories